

Light-induced large and tunable valley-selective Hall effect in a centrosymmetric system

Naoya Arakawa^{1,*} and Kenji Yonemitsu^{1,2}

¹The Institute of Science and Engineering, Chuo University, Bunkyo, Tokyo, 112-8551, Japan

²Department of Physics, Chuo University, Bunkyo, Tokyo 112-8551, Japan

We propose that a large and tunable valley-selective Hall effect can be realized in a centrosymmetric system via light-induced breaking of inversion and time-reversal symmetries. This is demonstrated in graphene driven by bicircularly polarized light, which consists of a linear combination of left- and right-handed circularly polarized light with different frequencies. We also show that our Hall conductivity is two orders of magnitude larger than the maximum value obtained in non-centrosymmetric systems, and that the main valley can be switched by tuning a phase difference between the left- and right-handed circularly polarized light. Our results will enable us to generate and control the valley-selective Hall effect in centrosymmetric systems.

Introduction. Electron systems can get a valley degree of freedom with broken inversion symmetry. In epitaxial or bilayer graphene [1, 2] and some transition-metal dichalcogenides [3], electrons at the K and K' points in the momentum space have the valley degree of freedom. These systems are noncentrosymmetric because their lattices break inversion symmetry; this symmetry holds in centrosymmetric systems. The valley degree of freedom can be used to realize valleytronics phenomena. An example is the valley-selective Hall effect, in which the current from one of two valleys causes the charge current perpendicular to an electric field. This was experimentally observed in MoS₂ [4] or bilayer graphene [5] with resonant circularly polarized light (CPL), which excites an electron at one valley [6–9]. Another example is a valley-contrasting Hall effect [10], in which the electrons around different valleys generate opposite currents perpendicular to the electric field. This is distinct from the valley-selective Hall effect because in the latter the contribution from one valley is negligible. Since the valley degree of freedom can be utilized in similar ways to the spin degree of freedom in spintronics, valleytronics has opened new phenomena and applications utilizing it.

Bicircularly polarized light (BCPL) will provide a new way for generating and controlling the valley degree of freedom. BCPL is generated by a linear combination of left- and right-handed CPL [11] and described by $\mathbf{A}_{\text{BCPL}}(t) = (A_x(t) \ A_y(t))^T$ [e.g., see Figs. 1(a) and 1(b)], where

$$A_x(t) + iA_y(t) = A_0 e^{i\Omega t} + A_0 e^{-i(\beta\Omega t - \theta)}. \quad (1)$$

If A_0 is strong enough to be treated nonperturbatively, BCPL can break time-reversal symmetry and inversion symmetry [12, 13]. Therefore, BCPL could generate the valley degree of freedom. To treat such nonperturbative effects, we need to consider a system driven by BCPL using the Floquet theory [14, 15]. Since the Hamiltonian in this theory can be changed by varying parameters of $\mathbf{A}_{\text{BCPL}}(t)$, BCPL could also control the valley degree of freedom. However, a possibility of a BCPL-induced

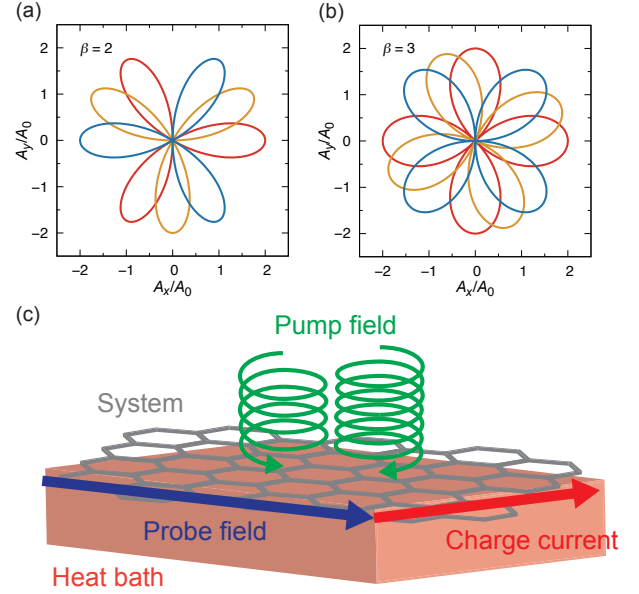


FIG. 1. (a), (b) Trajectories of $\mathbf{A}_{\text{BCPL}}(t)$ per period $T_p = 2\pi/\Omega$ for $\beta = 2$ and 3. The red, yellow, and blue lines correspond to those at $\theta = 0, \pi/2, \pi$, respectively. (c) The set-up for the valley-selective Hall effect in graphene driven by BCPL. The system, graphene, is driven by the pump field, the field of BCPL, and is weakly coupled to the heat bath. The charge current perpendicular to the probe field is generated.

valley-selective or valley-contrasting Hall effect remains unexplored.

Here we demonstrate the large and tunable valley-selective Hall effect in monolayer graphene driven by BCPL. Using a high-frequency expansion [16, 17] of the Floquet theory, we show that inversion symmetry can be broken only for even β in Eq. (1), whereas time-reversal symmetry can be broken for any β . We also show the effects of BCPL on the energy bands and the Berry curvatures. Then, using the Floquet linear-response theory [18–23], we show that the valley-selective Hall effect can be realized for $\beta = 2$ at $\theta = 0$ or π . Our Hall con-

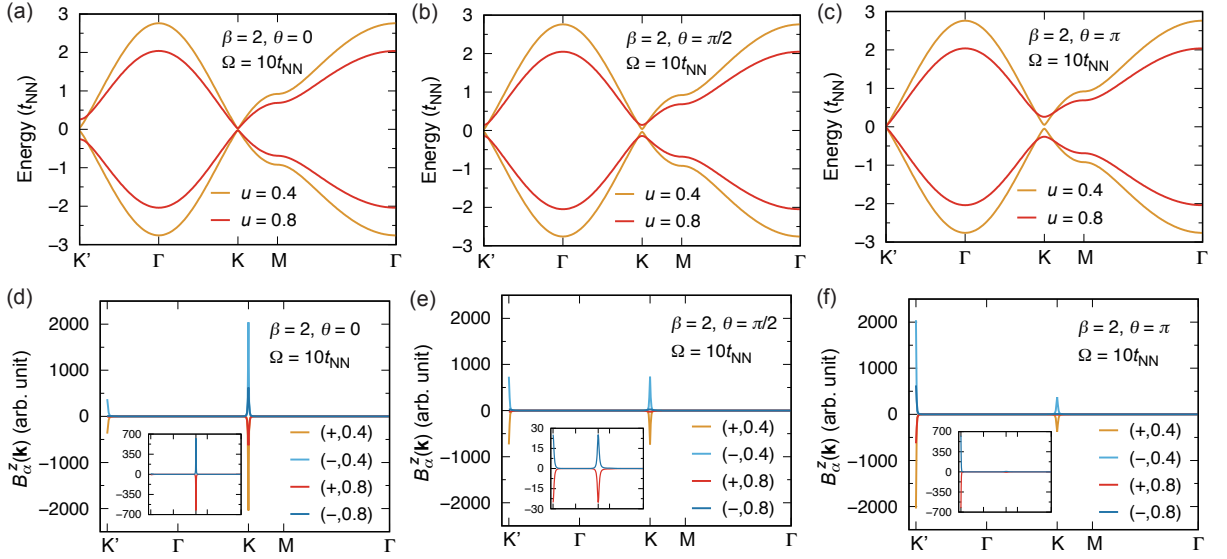


FIG. 2. (a)–(c) The momentum dependences of $\epsilon_+^{\text{eff}}(\mathbf{k})$ and $\epsilon_-^{\text{eff}}(\mathbf{k})$ obtained in the high-frequency expansion for $\beta = 2$ at $\Omega = 10t_{\text{NN}}$, $u = 0.4$ and 0.8 , and $\theta = 0, \frac{\pi}{2}$, and π . The momenta at the symmetric points K' , Γ , K , and M are $(\frac{8\pi}{3\sqrt{3}} 0)^T$, $(0, 0)^T$, $(\frac{4\pi}{3\sqrt{3}} 0)^T$, and $(\frac{\pi}{\sqrt{3}} \frac{\pi}{3})^T$, respectively. Here $(\frac{8\pi}{3\sqrt{3}} 0)^T$ and $(0, 0)^T$ are equivalent to $(-\frac{4\pi}{3\sqrt{3}} 0)^T$ and $(\frac{4\pi}{3\sqrt{3}} 0)^T$, respectively. (d)–(f) The momentum dependences of $B_\alpha^z(\mathbf{k})$ obtained in the high-frequency expansion for $\beta = 2$ at $\Omega = 10t_{\text{NN}}$ and $\theta = 0, \frac{\pi}{2}$, and π with $(\alpha, u) = (+, 0.4), (-, 0.4), (+, 0.8),$ and $(-, 0.8)$. The insets show the results for $u = 0.8$ on a smaller scale.

ductivity is much larger than the maximum value known so far, and the main valley can be switched by tuning θ . Our results indicate that BCPL can be used to generate and control the valley-selective Hall effect in centrosymmetric systems. This work will open the door to the valley-selective Hall effect in centrosymmetric systems.

Model. Graphene driven by BCPL [Fig. 1(c)] is described by the Hamiltonian,

$$H = H_s(t) + H_b + H_{\text{sb}}, \quad (2)$$

where $H_s(t)$ is the system Hamiltonian for graphene with the BCPL field $\mathbf{A}_{\text{BCPL}}(t)$, H_b is the bath Hamiltonian, and H_{sb} is the system-bath Hamiltonian. We have treated the nonperturbative effects of the BCPL field as the Peierls phase factors of the kinetic energy [18, 20, 22, 23]. In addition to $H_s(t)$, we have considered H_b and H_{sb} [20–23], where the bath is Büttiker-type [24, 25] and in equilibrium at temperature T . The main effect of these Hamiltonians is to induce the damping Γ [21–23], which could be used to realize a nonequilibrium steady state under heating [26, 27] induced by BCPL. Throughout this paper, we set $\hbar = k_B = c = a_{\text{NN}} = 1$, where a_{NN} is the length between nearest neighbor sites.

Inversion or time-reversal symmetry breaking.—We begin with symmetry breaking induced by BCPL. Using the high-frequency expansion [16, 17] of the Floquet theory, we obtain an effective Hamiltonian for describing the

nonperturbative effects of off-resonant BCPL,

$$H_{\text{eff}} = \sum_{\mathbf{k}} \sum_{a,b=A,B} \sum_{\sigma=\uparrow,\downarrow} \bar{\epsilon}_{ab}(\mathbf{k}) c_{\mathbf{k}a\sigma}^\dagger c_{\mathbf{k}b\sigma}, \quad (3)$$

where

$$\bar{\epsilon}_{AA}(\mathbf{k}) = -\bar{\epsilon}_{BB}(\mathbf{k}) = \Delta_{\text{BCPL}} + K_{AA}^{(\text{eff})}(\mathbf{k}), \quad (4)$$

$$\bar{\epsilon}_{AB}(\mathbf{k}) = \bar{\epsilon}_{BA}(\mathbf{k})^* = \epsilon_{AB}^{(\text{eff})}(\mathbf{k}). \quad (5)$$

(For the derivation, see the Supplemental Material [28].) Here Δ_{BCPL} is the staggered sublattice potential [12, 29, 30], $\epsilon_{AB}^{(\text{eff})}(\mathbf{k}) = \sum_{\mathbf{R}=\mathbf{R}_0, \mathbf{R}_1, \mathbf{R}_2} t_{\text{eff}}^{(AB)}(\mathbf{R}) e^{-i\mathbf{k}\cdot\mathbf{R}}$, and $K_{AA}^{(\text{eff})}(\mathbf{k}) = \sum_{\mathbf{R}=\pm\mathbf{R}'_0, \pm\mathbf{R}'_1, \pm\mathbf{R}'_2} K_{\text{eff}}^{(AA)}(\mathbf{R}) e^{-i\mathbf{k}\cdot\mathbf{R}}$, where $t_{\text{eff}}^{(AB)}(\mathbf{R})$ and $K_{\text{eff}}^{(AA)}(\mathbf{R})$ are the nearest-neighbor and next-nearest-neighbor hopping integrals, respectively. Note that $\mathbf{R}_0 = (0 1)^T$, $\mathbf{R}_1 = (-\frac{\sqrt{3}}{2} -\frac{1}{2})^T$, $\mathbf{R}_2 = (\frac{\sqrt{3}}{2} -\frac{1}{2})^T$, $\mathbf{R}'_0 = (\sqrt{3} 0)^T$, $\mathbf{R}'_1 = (-\frac{\sqrt{3}}{2} \frac{3}{2})^T$, and $\mathbf{R}'_2 = (-\frac{\sqrt{3}}{2} -\frac{3}{2})^T$ (see Fig. 1 of the Supplemental Material [28]). Equations (3)–(5) show that BCPL not only modifies the nearest-neighbor hopping integrals, but also induces the staggered sublattice potential and the next-nearest-neighbor hopping integrals. The latter quantities depend on β [see Eqs. (34) and (35) in the Supplemental Material [28]]; for even β , Δ_{BCPL} is finite and $K_{\text{eff}}^{(AA)}(\mathbf{R})$ has real and imaginary parts; for odd β , Δ_{BCPL} is zero and $K_{\text{eff}}^{(AA)}(\mathbf{R})$ is pure-imaginary. As specific cases, we show them for $\beta = 2$ and 3 in $u = eA_0 \ll 1$ (for their

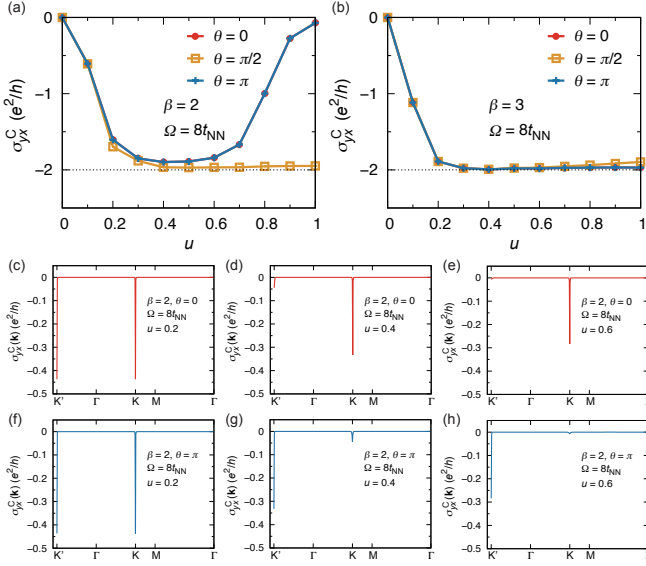


FIG. 3. (a), (b) The u dependences of σ_{yx}^C obtained in the Floquet linear-response theory for $\beta = 2$ or 3 at $\Omega = 8t_{\text{NN}}$ and $\theta = 0, \frac{\pi}{2},$ and π . Here $u = eA_0$ is dimensionless. The dotted lines correspond to a quantized value $-2e^2/h$. (c)–(h) The momentum dependences of $\sigma_{yx}^C(\mathbf{k})$ obtained in the Floquet linear-response theory for $\beta = 2$ at $\Omega = 8t_{\text{NN}}$ with $(\theta, u) = (0, 0.2), (0, 0.4), (0, 0.6), (\pi, 0.2), (\pi, 0.4),$ and $(\pi, 0.6)$. The symmetric points are the same as those used in Fig. 2.

derivation, see the Supplemental Material [28]):

$$\Delta_{\text{BCPL}} = \begin{cases} -6K_1(u, \theta) & (\beta = 2), \\ 0 & (\beta = 3), \end{cases} \quad (6)$$

$$K_{\text{eff}}^{(AA)}(\pm \mathbf{R}_l') = \begin{cases} \mp iK_0(u) + K_1(u, \theta) & (\beta = 2), \\ \mp i[K_0'(u) + K_{l+1}'(u, \theta)] & (\beta = 3), \end{cases} \quad (7)$$

where $K_0(u) = \frac{\sqrt{3}t_{\text{NN}}^2}{4\Omega}u^2$, $K_1(u, \theta) = \frac{t_{\text{NN}}^2}{4\Omega}u^3 \cos \theta$, $K_0'(u) = \frac{\sqrt{3}t_{\text{NN}}^2}{4\Omega}(u^2 - \frac{3}{4}u^4)$, $K_1'(u, \theta) = \frac{\sqrt{3}t_{\text{NN}}^2}{16\Omega}u^4 \cos \theta$, $K_2'(u, \theta) = \frac{t_{\text{NN}}^2}{16\Omega}u^4[\sin \theta - \sin(\theta - \frac{4\pi}{3})]$, and $K_3'(u, \theta) = -\frac{t_{\text{NN}}^2}{16\Omega}u^4[\sin \theta - \sin(\theta - \frac{2\pi}{3})]$. Therefore, BCPL can break inversion symmetry only for even β because it is broken by Δ_{BCPL} and the real parts of the next-nearest-neighbor hopping integrals. Furthermore, since time-reversal symmetry is broken by the imaginary parts of the next-nearest-neighbor hopping integrals [22, 31, 32], BCPL can break it for any β . Note that the l -independent $K_{\text{eff}}^{(AA)}(\pm \mathbf{R}_l')$'s for $\beta = 2$ preserve C_3 rotational symmetry, whereas the l -dependent ones for $\beta = 3$ break it.

Valley degeneracy lifting. The above differences between the effects of BCPL for even and odd β lead to a difference in the valley degeneracy. The energy dispersion of Eq. (3) is given by

$$\epsilon_{\pm}^{(\text{eff})}(\mathbf{k}) = \pm \sqrt{[\Delta_{\text{BCPL}} + K_{AA}^{(\text{eff})}(\mathbf{k})]^2 + |\epsilon_{AB}^{(\text{eff})}(\mathbf{k})|^2}. \quad (8)$$

We estimate $\epsilon_{\pm}^{(\text{eff})}(\mathbf{k})$'s at the K and K' points for $\beta = 2$ and 3 in $u \ll 1$; the results for $\beta = 2$ are $\epsilon_{\pm}^{(\text{eff})}(\mathbf{k}_K) = \pm|3\sqrt{3}K_0(u) - 9K_1(u, \theta)|$ and $\epsilon_{\pm}^{(\text{eff})}(\mathbf{k}_{K'}) = \pm|3\sqrt{3}K_0(u) + 9K_1(u, \theta)|$, where $\mathbf{k}_K = (\frac{4\pi}{3\sqrt{3}} 0)^T$ and $\mathbf{k}_{K'} = (\frac{8\pi}{3\sqrt{3}} 0)^T$; those for $\beta = 3$ are $\epsilon_{\pm}^{(\text{eff})}(\mathbf{k}_K) = \epsilon_{\pm}^{(\text{eff})}(\mathbf{k}_{K'})$. Therefore, the valley degeneracy can be lifted for even β due to a combination of breaking both time-reversal symmetry and inversion symmetry, whereas it is preserved for odd β .

The energy difference between the two valleys, $\Delta_{\text{valley}} = |\epsilon_{\pm}^{(\text{eff})}(\mathbf{k}_K) - \epsilon_{\pm}^{(\text{eff})}(\mathbf{k}_{K'})|$, for $\beta = 2$ can be controlled by changing u and θ . Figures 2(a)–2(c) show the θ dependence of $\epsilon_{\pm}^{(\text{eff})}(\mathbf{k})$ numerically calculated for $\beta = 2$ at $\Omega = 10t_{\text{NN}}$ and $u = 0.4$ and 0.8 . (For details of the numerical calculations, see the Supplemental Material [28].) At $\theta = 0$ and π , Δ_{valley} is finite and increases with increasing u [see Figs. 2(a) and 2(c)]. This is because $K_0(u)$ and $|K_1(u, \theta)|$ increase with increasing u . The valley which has the larger gap can be switched by changing θ from 0 to π or vice versa [compare Figs. 2(a) and 2(c)]. Meanwhile, at $\theta = \frac{\pi}{2}$, $\Delta_{\text{valley}} = 0$, i.e., the valley degeneracy holds [see Fig. 2(b)]. This is because $K_1(u, \theta) \propto \cos \theta$.

Valley-selective Hall effect. We turn to the nonperturbative effects of BCPL on the Berry curvatures for the driven system described by Eq. (3) for $\beta = 2$. The Berry curvature for the upper or lower band, $B_{\pm}^z(\mathbf{k})$ or $B_{\mp}^z(\mathbf{k})$, is given by

$$B_{\pm}^z(\mathbf{k}) = -i \frac{v_{\pm\mp}^x(\mathbf{k})v_{\mp\pm}^y(\mathbf{k}) - v_{\mp\mp}^y(\mathbf{k})v_{\pm\pm}^x(\mathbf{k})}{[\epsilon_{+}^{(\text{eff})}(\mathbf{k}) - \epsilon_{-}^{(\text{eff})}(\mathbf{k})]^2}, \quad (9)$$

where $v_{\alpha\beta}^{\nu}(\mathbf{k}) = \sum_{a,b=A,B} (U_{\mathbf{k}}^{\dagger})_{\alpha a} v_{ab}^{(\text{eff})\nu}(\mathbf{k}) (U_{\mathbf{k}})_{b\beta}$ ($\alpha, \beta = +, -$ and $\nu = x, y$), $(U_{\mathbf{k}})_{\alpha\alpha}$ is the unitary matrix to diagonalize Eq. (3), and $v_{ab}^{(\text{eff})\nu}(\mathbf{k}) = \frac{\partial \epsilon_{ab}(\mathbf{k})}{\partial k_{\nu}}$. Figures 2(d)–2(f) show the θ dependences of $B_{+}^z(\mathbf{k})$ and $B_{-}^z(\mathbf{k})$ numerically calculated for $\beta = 2$ at $\Omega = 10t_{\text{NN}}$ and $u = 0.4$ and 0.8 . (For details of the numerical calculations, see the Supplemental Material [28].) If the valley degeneracy is lifted (i.e., θ is 0 or π), the Berry curvatures at the two valleys are different in magnitude. The valley which gives the largest contribution to the Berry curvatures can be switched by changing θ from 0 to π or vice versa. These results suggest that BCPL could induce the valley-selective Hall effect and switch its dominant valley by changing θ . Furthermore, by changing θ from 0 or π to $\frac{\pi}{2}$ or vice versa, a crossover between the valley-selective and valley-independent Hall effects could be induced. However, even with broken inversion symmetry, the Berry curvatures of the upper or lower band at the two valleys have the same sign, which means the absence of the valley-contrasting Hall effect.

The results shown above are consistent with the time-averaged anomalous Hall conductivity (AHC) σ_{yx}^C calculated in the Floquet linear-response theory [18–23].

Figure 3(a) or 3(b) shows σ_{yx}^C numerically calculated at $\Omega = 8t_{\text{NN}}$ for $\beta = 2$ or 3. (For details of the numerical calculations, see the Supplemental Material [28].) For $\beta = 3$, σ_{yx}^C is quantized in a similar way to that of graphene driven by CPL [18, 22, 32]. This agrees with the analyses using the high-frequency expansion because the effective Hamiltonian for $\beta = 3$ is qualitatively the same as that of graphene driven by CPL [22, 32]. Meanwhile, for $\beta = 2$, σ_{yx}^C is quantized at $\theta = \frac{\pi}{2}$, whereas that is reduced from the quantized value for moderately large u 's at $\theta = 0$ and π . The magnitude reduction in σ_{yx}^C for large u 's at $\theta = 0$ or π is attributed to a drastic reduction in the contributions near one valley due to a larger gap opening. In all the cases, $\sigma_{yx}^C \approx -\sigma_{xy}^C$ is satisfied (see Fig. 2 in the Supplemental Material [28]). (Because of this, it is reasonable to call σ_{yx}^C the anomalous Hall conductivity.) Since such an antisymmetric part $(\sigma_{yx}^C - \sigma_{xy}^C)/2$ is finite only with broken time-reversal symmetry [33, 34], these results indicate that time-reversal symmetry is broken in all the cases, which agrees with the high-frequency expansion.

Then, Figs. 3(c)–3(h) show $\sigma_{yx}^C(\mathbf{k})$'s calculated in the Floquet linear-response theory for $\beta = 2$ at $\Omega = 8t_{\text{NN}}$ with $(\theta, u) = (0, 0.2), (0, 0.4), (0, 0.6), (\pi, 0.2), (\pi, 0.4),$ and $(\pi, 0.6)$, where $\sigma_{yx}^C(\mathbf{k})$ is defined as $\sigma_{yx}^C = \sum_{\mathbf{k}} \sigma_{yx}^C(\mathbf{k})$. For $u = 0.2$, $\sigma_{yx}^C(\mathbf{k}_K)$ and $\sigma_{yx}^C(\mathbf{k}_{K'})$ are almost the same. Meanwhile, for $u = 0.4$ and 0.6 , the main contribution at $\theta = 0$ or π comes from the vicinity at the K or K' point, respectively. These results indicate that moderately strong BCPL can induce the valley-selective Hall effect, and that the valley which gives the main contribution to this Hall effect can be switched by changing θ from 0 to π or vice versa. In contrast, $\sigma_{yx}^C(\mathbf{k}_K)$ and $\sigma_{yx}^C(\mathbf{k}_{K'})$ are degenerate at $\theta = \frac{\pi}{2}$ even for $u = 0.4$ and 0.6 (see Fig. 3 in the Supplemental Material [28]); the same degeneracy holds for $\beta = 3$ at $\theta = 0, \frac{\pi}{2},$ and π (see Fig. 3 in the Supplemental Material [28]). Therefore, by changing θ for $\beta = 2$, the crossover between the valley-selective and valley-independent Hall effects can be induced. Since the valley degeneracy is lifted only without both time-reversal symmetry and inversion symmetry, these results indicate that inversion symmetry is broken for even β at $\theta = 0$ and π , which also agrees with the high-frequency expansion.

Similar results are obtained at $\Omega = 6t_{\text{NN}}$ (see Fig. 4 in the Supplemental Material [28]), implying that the similar properties hold even in the resonant case. Therefore, our valley-selective Hall effect could be experimentally observed because for graphene driven by CPL, the results obtained in the Floquet linear-response theory [18, 22] are qualitatively reproducible in experiments using a smaller light frequency [35]. Note that the Floquet linear-response theory can analyze the off-resonant case and the resonant case, whereas the high-frequency expansion can analyze only the former case. Our light is resonant or

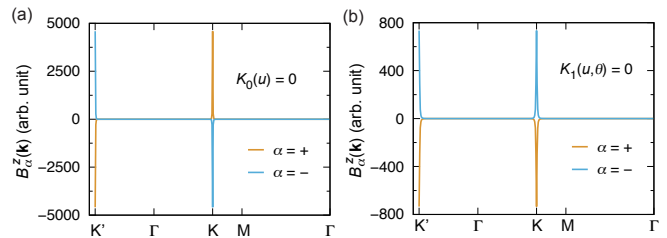


FIG. 4. (a), (b) The momentum dependences of $B_+^z(\mathbf{k})$ and $B_-^z(\mathbf{k})$ in the special cases with $K_0(u) = 0$ and $K_1(u, \theta) = 0$. The symmetric points are the same as those used in Fig. 2.

off-resonant if $\Omega \leq W_{\text{band}}$ or $\Omega > W_{\text{band}}$, respectively, where $W_{\text{band}} = 6t_{\text{NN}}$ is the bandwidth of the nondriven system.

Discussion. To understand why the valley-contrasting Hall effect is absent, we compare the Berry curvatures calculated for $\beta = 2$ using the high-frequency expansion with those in two special cases. In these cases, the effective Hamiltonian is given by Eq. (3) for $\beta = 2$ with $K_0(u) = 0$ or $K_1(u, \theta) = 0$, and the other parameters are the same as those used for $\beta = 2$ and $\Omega = 10t_{\text{NN}}$ at $\theta = 0$ and $u = 0.4$. Since the $K_0(u)$ term and $K_1(u, \theta)$ terms break time-reversal symmetry and inversion symmetry, respectively [Eqs. (6) and (7)], the first case possesses time-reversal symmetry, whereas the other possesses inversion symmetry. (The first case is similar to that studied in Ref. 10.) Note that for $\beta = 2$, $K_1(u, \theta)$ appears in Δ_{BCPL} and $K_{\text{eff}}^{(AA)}(\pm \mathbf{R}'_i)$ [Eqs. (6) and (7)]. Figures 4(a) and 4(b) show the Berry curvatures numerically calculated in these two cases. The Berry curvatures of the upper or lower band at the two valleys are opposite in sign with time-reversal symmetry. Therefore, we conclude that the valley-contrasting Hall effect is absent in graphene driven by BCPL due to the broken time-reversal symmetry. Note that the difference between the signs of the Berry curvatures at the two valleys without and with time-reversal symmetry may be similar to that between a ferromagnet and an antiferromagnet.

We compare our study with the relevant studies. The BCPL-induced symmetry breaking has been partly clarified in some off-resonant cases at $\beta = 2$ using the high-frequency expansion [12, 13]. Meanwhile, our results obtained in the high-frequency expansion are applicable to any β . Furthermore, our Floquet linear-response theory showed that these results remain qualitatively unchanged at smaller light frequencies including a resonant one for $\beta = 2$ and 3. Therefore, our results have a wider applicability. Then, there is no previous study showing the valley-selective Hall effect via the light-induced inversion symmetry breaking, although there are many studies about valley-dependent properties of periodically driven systems [36–41]. Therefore, our study is the first work demonstrating the BCPL-induced valley-selective Hall effect.

We also comment on three advantages of our valley-selective Hall effect. In the standard mechanism [4, 5], the inversion symmetry is broken by the lattice and the time-reversal symmetry is broken by resonant CPL. Meanwhile, in our mechanism, these symmetries are both broken by BCPL. Therefore, only our mechanism works in centrosymmetric systems. In addition, our mechanism enables us to switch the main valley and induce the crossover between the valley-selective and valley-independent Hall effects by tuning θ . Note that in the standard mechanism, the main valley can be switched by changing the helicity of CPL. Then, our Hall conductivity, which is $O(e^2/h)$ [e.g., see the value at $u = 0.6$ and $\theta = 0$ in Fig. 3(a)], is two orders of magnitude larger than the maximum value obtained in the standard mechanism [5]. This comes from a special property of monolayer graphene that the energy gaps at the two valleys are tunable solely by light, which enables us to make the energy gap at one valley much larger than the other with keeping the other small. Therefore, monolayer graphene driven by BCPL may provide the best opportunity for the valley-selective Hall effect.

* arakawa@phys.chuo-u.ac.jp

- [1] S. Y. Zhou et al., Substrate-induced bandgap opening in epitaxial graphene. *Nat. Mater.* **6**, 770-775 (2007).
- [2] T. Ohta, A. Bostwick, T. Seyller, K. Horn, and E. Rotenberg, Controlling the electronic structure of bilayer graphene. *Science* **313**, 951 (2006).
- [3] D. Xiao, G.-B. Liu, W. Feng, X. Xu, and W. Yao, Coupled spin and valley physics in monolayers of MoS₂ and other group-VI dichalcogenides. *Phys. Rev. Lett.* **108**, 196802 (2012).
- [4] K. F. Mak, K. L. McGill, J. Park, and P. L. McEuen, The valley Hall effect in MoS₂ transistors. *Science* **344**, 1489 (2014).
- [5] J. Yin et al., Tunable and giant valley-selective Hall effect in gapped bilayer graphene. *Science* **375**, 1398 (2022).
- [6] W. Yao, D. Xiao, and Q. Niu, Valley-dependent optoelectronics from inversion symmetry breaking. *Phys. Rev. B* **77**, 235406 (2008).
- [7] T. Cao et al., Valley-selective circular dichroism of monolayer molybdenum disulphide. *Nat. Commun.* **3**, 887 (2012).
- [8] H. Zeng, J. Dai, W. Yao, D. Xiao, and X. Cui, Valley polarization in MoS₂ monolayers by optical pumping. *Nature Nanotech.* **7**, 490–493 (2012).
- [9] K. F. Mak, K. He, J. Shan, and T. F. Heinz, Control of valley polarization in monolayer MoS₂ by optical helicity. *Nature Nanotech.* **7**, 494–498 (2012).
- [10] D. Xiao, W. Yao, and Q. Niu, Valley-contrasting physics in graphene: Magnetic moment and topological transport. *Phys. Rev. Lett.* **99**, 236809 (2007).
- [11] O. Kfir et al., Generation of bright phase-matched circularly-polarized extreme ultraviolet high harmonics. *Nat. Photonics* **9**, 99 (2015).
- [12] T. Nag, R.-J. Slager, T. Higuchi, and T. Oka, Dynamical synchronization transition in interacting electron systems. *Phys. Rev. B* **100**, 134301 (2019).
- [13] T. V. Trevisan, P. V. Arribi, O. Heinonen, R.-J. Slager, and P. P. Orth, Bicircular light Floquet engineering of magnetic symmetry and topology and its application to the Dirac semimetal Cd₃As₂. *Phys. Rev. Lett.* **128**, 066602 (2022).
- [14] J. H. Shirley, Solution of the Schrödinger equation with a Hamiltonian periodic in time. *Phys. Rev.* **138**, B979 (1965).
- [15] H. Sambe, Steady states and quasienergies of a quantum-mechanical system in an oscillating field. *Phys. Rev. A* **7**, 2203 (1973).
- [16] A. Eckardt and E. Anisimovas, High-frequency approximation for periodically driven quantum systems from a Floquet-space perspective. *New J. Phys.* **17**, 093039 (2015).
- [17] M. Bukov, L. D'Alessio, and A. Polkovnikov, Universal high-frequency behavior of periodically driven systems: From dynamical stabilization to Floquet engineering. *Adv. Phys.* **64**, 139 (2015).
- [18] T. Oka and H. Aoki, Photovoltaic Hall effect in graphene. *Phys. Rev. B* **79**, 081406(R) (2009).
- [19] M. Eckstein and M. Kollar, Theory of time-resolved optical spectroscopy on correlated electron systems. *Phys. Rev. B* **78**, 205119 (2008).
- [20] N. Arakawa and K. Yonemitsu, Light-induced mirror symmetry breaking and charge transport. unpublished (under review in *Phys. Rev. B*).
- [21] N. Tsuji, T. Oka, and H. Aoki, Nonequilibrium steady state of photoexcited correlated electrons in the presence of dissipation. *Phys. Rev. Lett.* **103**, 047403 (2009).
- [22] T. Mikami et al., Brillouin-Wigner theory for high-frequency expansion in periodically driven systems: Application to Floquet topological insulators. *Phys. Rev. B* **93**, 144307 (2016).
- [23] N. Arakawa and K. Yonemitsu, Symmetry-protected difference between spin Hall and anomalous Hall effects of a periodically driven multiorbital metal. *Commun. Phys.* **6**, 43 (2023).
- [24] M. Büttiker, Small normal-metal loop coupled to an electron reservoir. *Phys. Rev. B* **32**, 1846(R) (1985).
- [25] M. Büttiker, Role of quantum coherence in series resistors. *Phys. Rev. B* **33**, 3020 (1986).
- [26] L. D'Alessio and M. Rigol, Long-time behavior of isolated periodically driven interacting lattice systems. *Phys. Rev. X* **4**, 041048 (2014).
- [27] A. Lazarides, A. Das, and R. Moessner, Equilibrium states of generic quantum systems subject to periodic driving. *Phys. Rev. E* **90**, 012110 (2014).
- [28] See the Supplemental Material for the derivations of Eqs. (3), (6), and (7), the details of the numerical calculations, and additional numerical results.
- [29] S. Gwo and C. K. Shih, Site-selective imaging in scanning tunneling microscopy of graphite: The nature of site asymmetry. *Phys. Rev. B* **47**, 13059(R) (1993).
- [30] C. L. Kane and E. J. Mele, Quantum spin Hall effect in graphene. *Phys. Rev. Lett.* **95**, 226801 (2005).
- [31] F. D. M. Haldane, Model for a quantum Hall effect without Landau levels: Condensed-matter realization of the “parity anomaly”. *Phys. Rev. Lett.* **61**, 2015 (1988).
- [32] T. Kitagawa, T. Oka, A. Brataas, L. Fu, and E. Demler, Transport properties of nonequilibrium systems under the application of light: Photoinduced quantum Hall in-

- sulators without Landau levels. *Phys. Rev. B* **84**, 235108 (2011).
- [33] L. Onsager, Reciprocal relations in irreversible processes. I. *Phys. Rev.* **37**, 405 (1931).
- [34] L. Onsager, Reciprocal relations in irreversible processes. II. *Phys. Rev.* **38**, 2265 (1931).
- [35] J. W. McIver et al., Light-induced anomalous Hall effect in graphene, *Nat. Phys.* **16**, 38–41 (2020).
- [36] A. Kundu, H. A. Fertig, and B. Seradjeh, Floquet-engineered valleytronics in Dirac systems. *Phys. Rev. Lett.* **116**, 016802 (2016).
- [37] M. S. Mrudul, Á. J.-Galán, M. Ivanov, and G. Dixit, Light-induced valleytronics in pristine graphene. *Optica* **8**, 422 (2021).
- [38] M. S. Mrudul and G. Dixit, Controlling valley-polarisation in graphene via tailored light pulses. *J. Phys. B: At. Mol. Opt. Phys.* **54**, 224001 (2021).
- [39] D. S. L. Abergel and T. Chakraborty, Generation of valley polarized current in bilayer graphene. *App. Phys. Lett.* **95**, 062107 (2009).
- [40] M. Tahir, Q. Y. Zhang, and U. Schwingenschlögl, Floquet edge states in germanene nanoribbons, *Sci. Rep.* **6**, 31821 (2016).
- [41] J. Mei, L. Shao, H. Xu, X. Zhu, and N. Xu, Photomodulated edge states and multiterminal transport in silicene-like nanoribbons, *Phys. Rev. B* **99**, 045444 (2019).

ACKNOWLEDGMENTS

This work was supported by JST CREST Grant No. JPMJCR1901, JSPS KAKENHI Grant No. JP22K03532, and MEXT Q-LEAP Grant No. JPMXS0118067426.